JOURNAL OF AIRCRAFT
Vol. 47, No. 4, July–August 2010

Helicopter Rotor Load Prediction Using a Geometrically Exact Beam with Multicomponent Model

Hyun-Ku Lee,* S. R. Viswamurthy,† Sang Chul Park,‡ Taeseong Kim,§ and Sang Joon Shin¶
Seoul National University, Seoul 151-742, Republic of Korea
and
Deog-Kwan Kim**
Korea Aerospace Research Institute, Daejeon 305-333, Republic of Korea

DOI: 10.2514/1.47608

In this paper, an accurate structural dynamic analysis was developed for a helicopter rotor system including rotor control components, which was coupled to various aerodynamic and wake models in order to predict an aeroelastic response and the loads acting on the rotor. Its blade analysis was based on an intrinsic formulation of moving beams implemented in the time domain. The rotor control system was modeled as a combination of rigid and elastic components. A multicomponent analysis was then developed by coupling the beam finite element model with the rotor control system model to obtain a complete rotor-blade/control-system aeroelastic analysis. The rotor blade analysis was in good agreement and validated by comparing with DYMORE. Numerical results were obtained for a four-bladed, small-scale, articulated rotor rotating in vacuum and in a wind tunnel to simulate forward-flight conditions and its aerodynamic effects. The complete rotor-blade/control-system model was loosely coupled with various inflow and wake models in order to simulate both hover and forward-flight conditions. The resulting rotor blade response and pitch link loads are in good agreement with those predicted by CAMRAD II. The present analysis features both model compactness and robustness in its solution procedure while capturing the sophisticated behavior of individual rotor components. The analysis is expected to be part of a framework useful in the preliminary design phase for helicopters.

Nomenclature

AC	=	orientation of the undeformed pitch link
b	=	undeformed beam reference frame
C	=	Rotation matrix, $C^{ab}C^{Ba}$
C^{ab}	=	transformation matrix from frame b to frame a
C^{Ba}	=	transformation matrix from frame a to frame B
e_1	=	unit vector, $[1, 0, 0]^T$
F	=	internal force vector
H	=	angular momentum vector
I_{ij}	=	elements of the 6×6 inertial matrix of each finite element ($I_{11}, I_{12}, \ldots, I_{66}$)
K	=	kinetic energy density per unit blade span
K_{ij}	=	elements of the 6×6 stiffness matrix of each finite element ($K_{11}, K_{12}, \ldots, K_{66}$)
k_{pl}, c_{pl}	=	stiffness and damping coefficients of the elastic pitch link
l_{pl}	=	length of the undeformed pitch link
M	=	internal moment vector
P	=	linear momentum vector
PC	=	orientation of the pitch horn
R	=	rotor radius
U	=	potential energy density per unit blade span
u	=	displacement vector
V	=	linear velocity vector
γ	=	force strain vector
$\underline{\Delta}$	=	3×3 identity matrix
$\overline{\delta A}$	=	virtual action at the ends of the rotor blade and at the ends of the time interval
δW	=	virtual work of externally applied loads per unit length
θ	=	rotation vector expressed in terms of Rodrigues parameters
$\tilde{\theta}$	=	operator converts a column vector to its dual matrix
κ	=	moment strain vector
Ω	=	angular velocity vector

Received 11 October 2009; revision received 13 March 2010; accepted for publication 27 March 2010.

*Graduate Student, Currently Research Engineer, Hyundai Motor Company, Gyeonggi-Do, Republic of Korea.
†Postdoctoral Fellow; Currently Scientist, National Aerospace Laboratories, Bangalore, India.
‡Graduate Student, School of Mechanical and Aerospace Engineering.
§Postdoctoral Fellow; currently Research Scientist, Risø DTU, Roskilde, Denmark.
¶Associate Professor, Institute of Advanced Aerospace Technology, School of Mechanical and Aerospace Engineering, 599 Gwanangno, Gwanak-gu (Corresponding Author).
**Research Engineer, Rotor Division.

I. Introduction

HELICOPTERS operate in many different flight regimes and are sometimes required to conduct extreme maneuvers. Prediction of the rotor system component loads is therefore important even in the early phase of design. Helicopter rotor blades are long, slender and generally undergo moderate to large displacements due to aerodynamic loads. Also, the aerodynamic environment around the rotor is highly unsteady and complex [1,2]. To make accurate predictions for the rotor blade, hub and control component loads, a sophisticated aeroelastic analysis is required for related helicopter rotor systems. Industry, research institutes, and academia have developed a few comprehensive aeroelastic analyses for that purpose. Existing analyses such as the Comprehensive Analytical Model of Rotorcraft Aerodynamics and Dynamics (CAMRAD II) [3,4], University of Maryland Advanced Rotorcraft Code (UMARC) [5], and DYMORE [6] have been widely used to predict helicopter aeroelastic response accurately.

CAMRAD II is one of the most advanced comprehensive rotorcraft analyses and predicts performance, trim, stability, and loads. In its structural analysis, component rigid body motion is assumed to be large, and the kinematics of the interfaces and rigid body motion are treated in an exact manner. For rotor structures, three different models are provided regarding the geometrical non-

linearity: exact beam, almost-exact beam, and second-order approximated beam [7]. In aerodynamics, it implements a lifting-line theory using two-dimensional steady airfoil characteristics and a vortex wake. For an unsteady airfoil motion, various levels of unsteady aerodynamic models and dynamic stall models are provided [8]. However, it requires a significant amount of detailed input parameters in order to establish a correct trim condition and obtain pertinent results. Thus, CAMRAD II may not be an appropriate numerical analysis, especially at a preliminary design stage of a helicopter.

UMARC is one of the existing comprehensive programs for aeroelastic analysis of a helicopter rotor and is based on the finite element methodology. UMARC uses a geometrically nonlinear but approximated beam formulation, which only retains the terms up to the second order based on an ordering scheme [9]. Datta and Chopra [10] used UH-60A flight-test data to validate the structural and aerodynamic models included in UMARC. The lower harmonic torsional moments and pitch link loads were well predicted, though deficiencies existed for torsion loads above 4/rev. They found that the predictions were sensitive to the particular wake model used and the trim state. Datta and Chopra also attempted to couple the helicopter structural dynamics model in UMARC with a separate computational fluid dynamics (CFD) analysis to predict the vibratory loads in a high-speed flight [11]. They reported that CFD and computational structural dynamics (CSD) coupling improved the prediction for torsional loads. The peak-to-peak and lower harmonics of the pitch link load were captured well. However, they found that the higher harmonic components in the pitch link loads were not captured well. The discrepancies in the predicted higher harmonic torsion loads remained even when CFD analysis was replaced by the measured aerodynamic loads, which were obtained from the UH-60A Airloads Program. The discrepancy was attributed to the limitations in the structural dynamic model of the helicopter rotor. Use of a geometrically exact beam formulation is suggested as one of the remedies to overcome such limitations.

Bauchau [12,13] developed a finite element program called DYMORE for the analysis of a nonlinear flexible multibody system. DYMORE implements a nonlinear finite element analysis, and its element library includes rigid and deformable bodies as well as various joint elements. The element library includes rigid bodies, cables, beams, and shells. Joints can be modeled as planar, cylindrical, screw, revolute, spherical, and prismatic. The beam formulation in DYMORE is geometrically exact. An entire rotor system consisting of blades, pitch horns, pitch links, and the swashplate can be modeled in DYMORE and appropriate boundary conditions can also be established. The resulting nonlinear equations of the motion are then solved for the complete multibody system using an energy-decaying, time integration scheme, which is unconditionally stable [14]. References [15,16] use DYMORE to predict the aeroelastic response and stability of the helicopter rotors. However, DYMORE only provides a simple two-dimensional unsteady airfoil theory and a finite state dynamic inflow model to calculate the inflow velocity field over the rotor disk [17,18]. Also, a very detailed description is usually required for multibody degrees of freedom in DYMORE. This significantly increases the size of the matrices it needs to handle and often makes it difficult to interpret the eigenvalue results regarding aeroelastic stability.

In this paper, an improved structural dynamic analysis will be presented for helicopter rotor blade and control system components. And, then it will be combined with an appropriate aerodynamic model in order to make an accurate prediction of blade and pitch link loads for various flight conditions. The present structural analysis is intended to feature the following important aspects: compactness in its model size and sophistication for predicting blade and control loads accurately. Thus, it is expected to be a valuable design and analysis tool for the preliminary design phase of helicopters.

To construct a robust and precise aeroelastic analysis framework, an accurate structural dynamic analysis will be developed for a helicopter rotor system, which can then be coupled with various aerodynamic and wake models, ranging from the simple lifting-line theory to CFD. A complex three-dimensional structural analysis for a rotor blade will be separated into a set of two analyses: a linear analysis over the cross section and a nonlinear analysis of the blade reference axis. An approach based on the variational asymptotic method [19] considering the effects of curvature, twist and warping will be used to obtain the cross-sectional stiffness properties of anisotropic rotor blades. The elastic properties thus obtained will then be used in the one-dimensional beam analysis. The present structural analysis is derived based on the mixed variational formulation of moving beams suggested by Hodges [20]. Shang [21] implemented such formulation of a rotating beam in the frequency domain, and Cheng [22] further modified it to be implemented in the time domain. The rotor control system components will be modeled as a combination of rigid and elastic components. A multicomponent analysis will then be developed by coupling the blade analysis with the rotor control system model. This will be combined with suitable aerodynamic and wake models or CFD to predict the blade and control system loads. Numerical validation will be conducted for the structural and aerodynamic models developed. Then the aeroelastic response and loads will be validated by the coupling of the structural and aerodynamic models.

II. Geometrically Exact Beam Formulation

The nonlinear intrinsic formulation originally developed by Hodges [20] assumes small strains and finite rotations. It is applicable for slender beams like helicopter rotor blades that are initially curved and twisted. This formulation does not approximate the geometry of the deformed beam reference line and is therefore suitable for cases of large displacements and rotations.

The variational formulation is derived from Hamilton's principle, which can be written as

$$\int_{t_1}^{t_2}\int_0^R [\delta(K-U)+\delta W]\,\mathrm{d}x_1\,\mathrm{d}t = \overline{\delta A} \tag{1}$$

The internal force, internal moment, linear momentum, and angular momentum vectors in the deformed blade reference frame B are introduced as [20]

$$F_B = \left(\frac{\partial U}{\partial \gamma}\right)^T \quad M_B = \left(\frac{\partial U}{\partial \kappa}\right)^T \quad P_B = \left(\frac{\partial K}{\partial V_B}\right)^T \quad H_B = \left(\frac{\partial K}{\partial \Omega_B}\right)^T \tag{2}$$

With the above equations, Eq. (1) can be written as

$$\int_{t_1}^{t_2}\int_0^R [\delta V_B^{*T} P_B + \delta\Omega_B^{*T} H_B - \delta\gamma_B^{*T} F_B - \delta\kappa_B^{*T} M_B + \delta W]\,\mathrm{d}x_1\,\mathrm{d}t = \delta A \tag{3}$$

The superscript $*$ means that V_B^*, Ω_B^*, γ^*, and κ^* satisfy the kinematic equations, which ensure satisfaction of the geometric exactness as follows [20]:

$$\gamma = C^{Ba}(C^{ab}e_1 + u_a') - e_1 \qquad \kappa = C^{Ba}\left(\frac{\Delta - \frac{\tilde{\theta}}{2}}{1+\frac{\theta^T\theta}{2}}\right)\theta'$$

$$V_B = C^{Ba}(v_a + \dot{u}_a + \tilde{\omega}_a u_a) \qquad \Omega_B = C^{ba}\left(\frac{\Delta - \frac{\tilde{\theta}}{2}}{1+\frac{\theta^T\theta}{2}}\right)\dot{\theta} + C^{Ba}\omega_a \tag{4}$$

In a typical displacement-based formulation such as the one presented in [11], the kinematical equations are very long and cumbersome. Also, the numerical implementation of such formulation results in inaccuracies due to truncation of polynomial functions. An alternative to this approach is to combine the intrinsic beam formulation with the constitutive and kinematic relations [Eqs. (2) and (4), respectively] through the use of Lagrange multipliers, thereby maintaining the generalized displacements, strains, forces, and momenta as independent variables. Following the latter approach, Eq. (3) becomes

$$\int_{t_1}^{t_2}\int_0^R [\delta V_B^{*T} P_B + \delta\Omega_B^{*T} H_B - \delta\gamma_B^{*T} F_B - \delta\kappa_B^{*T} M_B + \delta F_B^T(\gamma-\gamma^*) + \delta M_B^T(\kappa-\kappa^*) - \delta P_B^T(V_B - V_B^*) - \delta H_B^T(\Omega_B - \Omega_B^*) + \delta W]\,\mathrm{d}x_1\,\mathrm{d}t = \delta A \tag{5}$$

Transforming the above equation to frame a using the rotation matrix C and performing integration by parts, the variational formulation based on exact intrinsic equations for moving beams in the hub rotating frame a can be written as

$$\int_{t_1}^{t_2} \delta\Pi_a\,\mathrm{d}t = 0 \tag{6}$$

where

$$\begin{aligned}\delta\Pi_a = \int_0^R \Big\{ & \delta u_a'^T C^T C^{ab} F_B + \delta u_a^T [(C^T C^{ab} P_B)^\bullet + \tilde{\omega}_a C^T C^{ab} P_B] \\ & + \overline{\delta\psi_a}'^T C^T C^{ab} M_B - \overline{\delta\psi_a}^T C^T C^{ab}(\tilde{e}_1 + \tilde{\gamma}) F_B \\ & + \overline{\delta\psi_a}^T [(C^T C^{ab} H_B)^\bullet + \tilde{\omega}_a C^T C^{ab} H_B + C^T C^{ab} \tilde{V}_B P_B] \\ & - \overline{\delta F_a}^T [C^T C^{ab}(\tilde{e}_1 + \tilde{\gamma}) - C^{ab} e_1] - \delta F_a'^T u_a \\ & - \overline{\delta M_a}^T \left(\Delta + \frac{\tilde{\theta}}{2} + \frac{\theta\theta^T}{4}\right) C^{ab}\kappa - \delta M_a'^T \theta \\ & + \overline{\delta P_a}^T (C^T C^{ab} V_B - v_a - \tilde{\omega}_a u_a) - \overline{\delta P_a}^T \dot{u}_a \\ & + \overline{\delta H_a}^T \left(\Delta - \frac{\tilde{\theta}}{2} + \frac{\theta\theta^T}{4}\right)(C^T C^{ab}\Omega_B - \omega_a) - \overline{\delta H_a}^T \dot{\theta} \\ & - \delta u_a^T f_a - \overline{\delta\psi_a}^T m_a \Big\}\,\mathrm{d}x_1 - (\delta u_a^T \hat{F}_a + \overline{\delta\psi_a}^T \hat{M}_a \\ & - \overline{\delta F_a}^T \hat{u}_a - \overline{\delta M_a}^T \hat{\theta})|_0^R \end{aligned} \tag{7}$$

In the above equation, f_a and m_a are the external force and moment vectors, respectively. The hatted terms are the boundary values of the corresponding quantities. The generalized strain and force measure and velocity and momentum measures are related through the constitutive laws in the following form:

$$\begin{Bmatrix} F_B \\ M_B \end{Bmatrix} = [K] \begin{Bmatrix} \gamma \\ \kappa \end{Bmatrix} \qquad \begin{Bmatrix} P_B \\ H_B \end{Bmatrix} = [M] \begin{Bmatrix} V_B \\ \Omega_B \end{Bmatrix} \tag{8}$$

Discretizing Eq. (6) in the spatial domain into N finite elements, the above equation can be reduced to the following:

$$\int_{t'}^{t_2} \sum_{i=1}^{N} \delta\Pi_i\,\mathrm{d}t = 0 \tag{9}$$

This results in a set of nonlinear governing equation as follows:

$$F_S(X, \dot{X}) - F_L = 0 \tag{10}$$

where F_S is a structural operator, F_L is an external load operator, and X is the unknown structural state variable vector organized as follows:

$$X = [\hat{F}_1^T \hat{M}_1^T u_1^T \theta_1^T F_1^T M_1^T P_1^T H_1^T \cdots u_N^T \theta_N^T F_N^T M_N^T P_N^T H_N^T \hat{u}_{N+1}^T \hat{\theta}_{N+1}^T]^T \tag{11}$$

where u is the displacement vector in the frame a, and θ is the rotation vector expressed in terms of the Rodrigues parameters. The hatted terms in the above expression are the boundary values of the corresponding quantities that depend on the boundary conditions. Equation (10) is a set of the first-order ordinary differential equations. The time derivative of the unknown vector X is calculated based on the variables during the previous two time steps, by using second-order backward Euler method. The problem is then converted to the solution of a set of nonlinear algebraic equations of the form

$$F_S(X^n) - F_L = 0 \tag{12}$$

where X^n is the unknown structural vector at time step n. Newton-Raphson method is used to solve the above set of nonlinear algebraic equations. The present structural analysis can be coupled with an appropriate aerodynamic model through the external load operator F_L. The unknown vector X will be modified slightly when considering an articulated rotor instead of a hingeless rotor.

III. Prediction of Loads in the Control System Components

The primary objective of this paper was to develop a CSD analysis that can be readily coupled with various analyses developed to model the aerodynamic environment of a helicopter rotor. In particular, the combined aeroelastic analysis was used to estimate the loads acting on the control system components of the helicopter.

The schematic of the rotor blade and control system is shown in Fig. 1. The rotor blade is modeled using the geometrically exact beam formulation described in Sec. II. The components of the rotor control system such as the pitch link, pitch horn, swashplate, and servo actuators are modeled as a combination of rigid and elastic bodies. A systematic approach was then followed to couple the rotor control system model with the beam finite element model to obtain a complete blade-control system model. Such unified structural model was developed in a modularized fashion so that it can then be easily coupled with the various aerodynamic and wake models or even CFD.

As a preliminary step, only the pitch horn, pitch link, and the rotating swashplate were considered in this paper. The pitch horn and the rotating swashplate are modeled as rigid bodies with negligible mass. The pitch link is modeled as a combination of an elastic linear spring and linear viscous damper. The additional terms in the virtual variation in the strain energy and virtual work expressions due to the elastic pitch link can be written as follows:

$$\delta U_{\mathrm{pl}} = k_{\mathrm{pl}} E_{\mathrm{pl}} \delta E_{\mathrm{pl}} \qquad \delta W_{\mathrm{pl}} = -c_{\mathrm{pl}} \dot{E}_{\mathrm{pl}} \delta E_{\mathrm{pl}} \tag{13}$$

where E_{pl} is the elongation of the pitch link. It is now assumed that the vertical motion of the swashplate (h_{sp}) is prescribed. Later, this motion will become a new degree of freedom when the swashplate is modeled as an elastic component. The deformed pitch link orientation $\mathbf{A'C'}$ is related to the swashplate motion and blade root motion as follows (Fig. 2):

$$\mathbf{A'C'} = -h_{\mathrm{sp}}\hat{k} + \mathbf{AC} + \mathbf{CP} + \mathbf{u}_{aP} + C_P^T \mathbf{PC} \tag{14}$$

where $\mathbf{u}_{aP}$ and C_P^T are the displacement and rotation of the pitch horn attachment point P and all the relevant quantities are measured in frame a. The elongation of the pitch link can then be written as

$$E_{\mathrm{pl}} = |\mathbf{A'C'}| - l_{\mathrm{pl}} \tag{15}$$

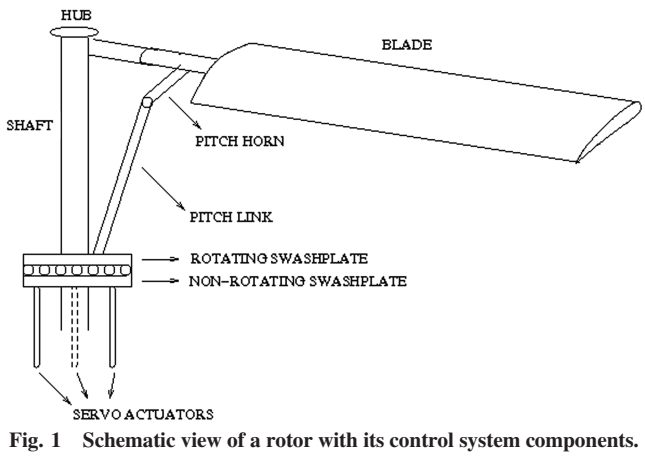

Fig. 1 Schematic view of a rotor with its control system components.

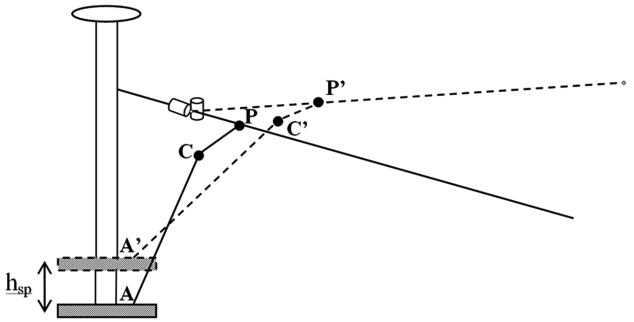

Fig. 2 Analysis of the control system components.

The above nonlinear equation provides the kinematic relationship between the pitch link elongation (E_{pl}) and motion of the blade root and swashplate motion. This nonlinear equation is used to obtain the expression for δE_{pl} in terms of the virtual displacements (δu_1, δu_2, and δu_3) and virtual rotations ($\delta\psi_1$, $\delta\psi_2$, and $\delta\psi_3$) at the pitch horn attachment point on the rotor blade P. From Eq. (15) we can write

$$\delta E_{\text{pl}} = E_{u1}\delta u_1^a + E_{u2}\delta u_2^a + E_{u3}\delta u_3^a + E_{\theta 1}\delta\psi_1^a + E_{\theta 2}\delta\psi_2^a + E_{\theta 3}\delta\psi_3^a \tag{16}$$

Since Eq. (15) is nonlinear, E_{u1}, E_{u2}, E_{u3}, $E_{\theta 1}$, $E_{\theta 2}$, and $E_{\theta 3}$ are not constants. Rather, they are functions of the displacements and rotations at P. The modified governing equations of the motion are obtained after adding the expressions for δU_{pl} and δW_{pl} to the original expression for δU and δW, respectively, in Eq. (1). The nonlinear algebraic equations are then solved to obtain the blade deformation and loads along with the deformation of the elastic pitch link. The loads acting on the pitch link and the rotating swashplate are then obtained from the above solution. In the future, it is the authors' plan to include an elastic model of the servo actuators and the inertial properties of the rotating and nonrotating swashplates.

The present approach increases the number of degrees of freedom in the structural model by only one per blade while capturing the behavior of the control linkages to a reasonable extent. Compared with the present model, control system modeling in a general multibody dynamics analysis, such as DYMORE, will increase the problem complexity appreciably due to the additional degrees of freedom introduced by the control linkages and joints.

IV. Validation of the Geometrically Exact Beam Formulation

To validate the geometrically exact beam analysis, a few test cases were numerically simulated using a computer program. The results from such test cases are presented here. A simple rotating beam clamped at the root and with a tip force acting along the a_3 direction, as shown in Fig. 3, is considered. The material properties of the simple beam are described in Table 1. The dynamic response of the beam was calculated using beam analysis and compared with the results obtained by DYMORE. Figures 4 and 5 show the comparison of the tip displacements and rotations under the application of a tip force equal to $50 \sin 20t$ N. Figures 6 and 7 show the root forces and moments for the case along with the results from DYMORE simulations. The time-step size used in both computer simulations was 1×10^{-3} s. It was seen that the two results are nearly identical except for the axial force component at the root, where the difference between the two analyses is less than 2%.

V. Numerical Results and Discussion

In this paper, a four-bladed small-scaled experimental rotor was used for numerical analysis. The properties of the small-scaled rotor are given in Table 2. The rotor blade is discretized into 10 finite elements along the spanwise direction. To validate the present analysis, a well-established rotorcraft comprehensive analysis program, CAMRAD II [5,6], was used. Modeling of an existing small-scaled experimental rotor and its relevant CAMRAD II input files were originally written and executed by the Korea Aerospace Research Institute. Those files were further modified and used in this paper.

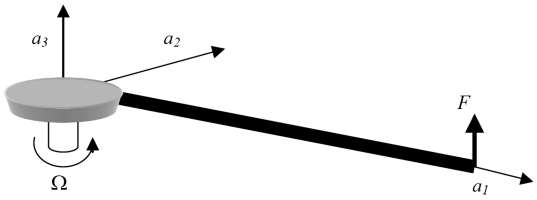

Fig. 3 Test case considered for validation of the exact beam analysis.

A. Small-Scaled Rotor Rotating in Vacuum

First, the small-scaled rotor was analyzed in a vacuum. Under the conditions of a vacuum since the aerodynamic loads are absent, the response of the rotor blade is simply due to the equilibrium between inertial and centrifugal forces. The results of the blade response in a vacuum predicted by the beam analysis coupled with a multicomponent model were compared with those obtained by CAMRAD II. Figure 8 shows the steady flapping response of the rotor blade predicted by the present analysis along with those obtained by CAMRAD II. The results obtained by the analysis are in good agreement with those by CAMRAD II. It should be noted that the blade tip flapwise deflection in case of the vacuum is quite small compared with the rotor radius. Figure 9 shows the blade feathering response in vacuum corresponding to a collective pitch setting of 1.30°. The prediction from the analysis is in good agreement with those from CAMRAD for the inboard and tip sections of the blade. However, the analysis overpredicts the feathering response near the midspan of the rotor blade.

B. Small-Scale Rotor Hovering in a Wind Tunnel

Next, the small-scale experimental rotor was analyzed under a hover condition in a wind tunnel. As a first step, the external loads were obtained from the aerodynamic analysis in CAMRAD II. A simple uniform inflow aerodynamics was chosen to analyze the effect of the rotor wake. The spanwise distribution of the sectional aerodynamic lift and pitching moment predicted by CAMRAD II are shown in Figs. 10 and 11. The above distributed aerodynamic loads are integrated over appropriate spanwise lengths and then applied as concentrated forces and moments at the nodes of the beam analysis. A comparison of the resulting steady flapwise deflection between the analysis and CAMRAD II is shown in Fig. 12. The analysis predicted

Table 1 Material properties of the test beam

Properties	Values
Mass per unit span	0.2 kg/m
I_{44}	10^{-4} kg · m
I_{55}	10^{-6} kg · m
I_{66}	10^{-4} kg · m
K_{11}	10^{6} N
K_{22}	10^{20} N
K_{33}	10^{20} N
K_{44}	50 N · m^2
K_{55}	50 N · m^2
K_{66}	1000 N · m^2

Table 2 Properties of the small-scale experimental rotor

Properties	Values
Rotor type	Articulated
Rotor radius	1.129 m
Number of blades	4
Rotor speed	199.38 rad/s

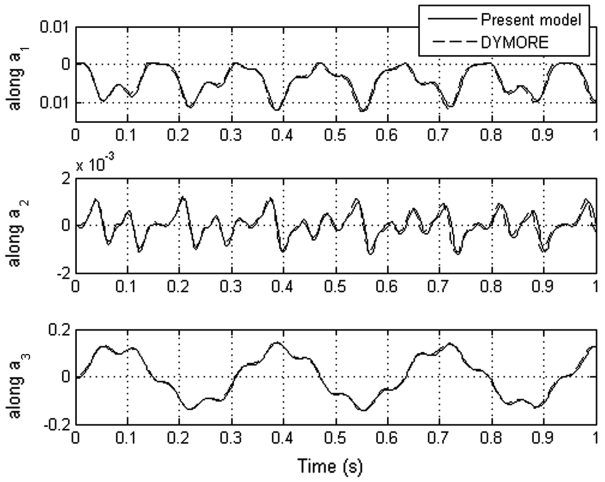

Fig. 4 Comparison of the tip displacements in the test beam.

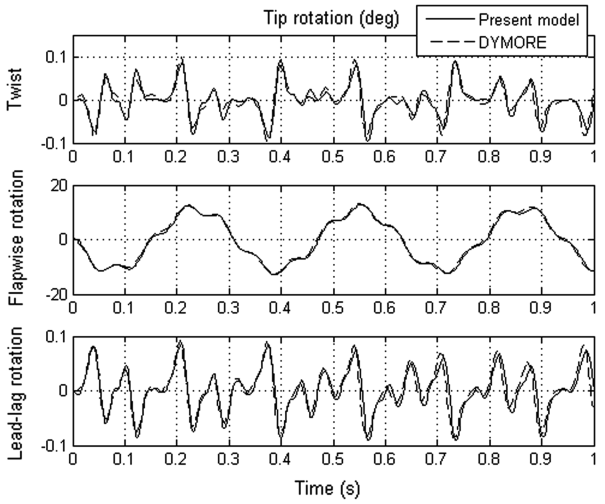

Fig. 5 Comparison of the tip rotations in the test beam.

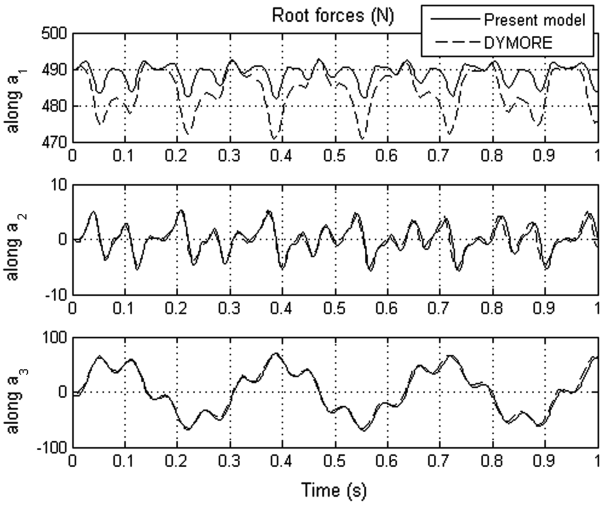

Fig. 6 Comparison of the root forces in the test beam.

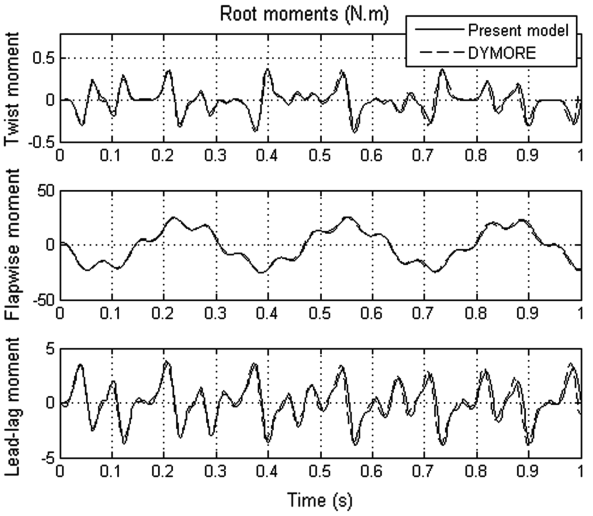

Fig. 7 Comparison of the root moments in the test beam.

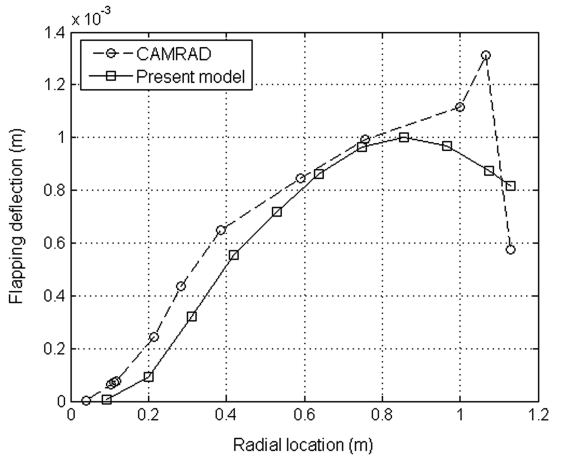

Fig. 8 Comparison of the blade flapwise response in a vacuum.

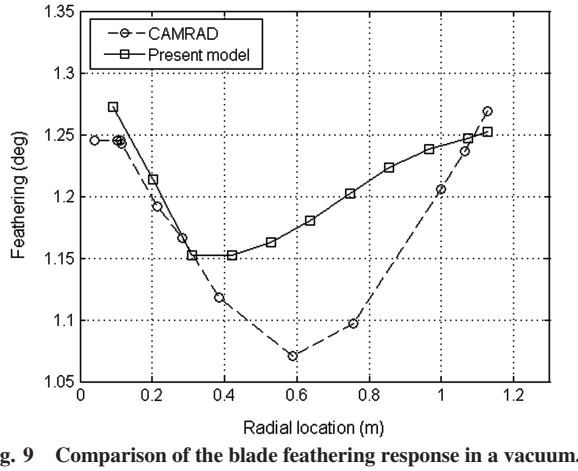

Fig. 9 Comparison of the blade feathering response in a vacuum.

a marginally higher flapwise deflection than CAMRAD II. Figure 13 shows the lead-lagging deflection of the rotor blade in hover. It is observed that the lead-lagging prediction from the present analysis is in good agreement with those by CAMRAD II. Figure 14 shows the blade feathering response in hover predicted by the analysis and CAMRAD II. A collective pitch of 1.30° is used for the simulation. The structural analysis developed in this paper captures the overall trend in the feathering response, but overpredicts the tip feathering response by about 0.4°.

In the next section, the unified rotor-blade/control-system structural model was combined with various aerodynamic and wake models to simulate hover and forward-flight conditions.

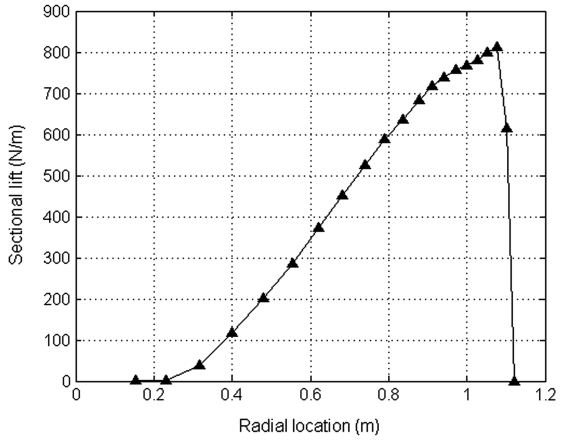

Fig. 10 Spanwise aerodynamic lift distribution in hover; collective pitch is 1.30°.

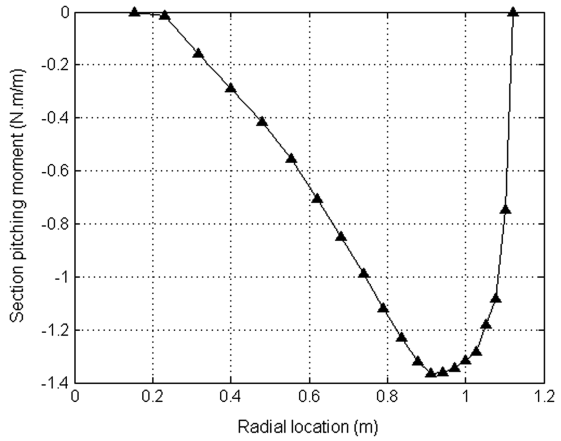

Fig. 11 Spanwise aerodynamic pitching moment distribution in hover; collective pitch is 1.30°.

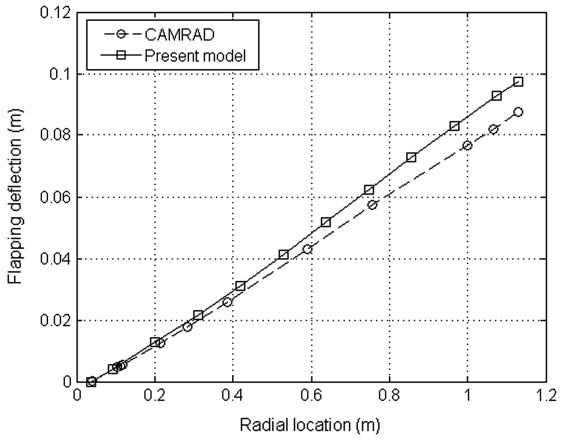

Fig. 12 Blade flapwise response in hover; collective pitch is 1.30°.

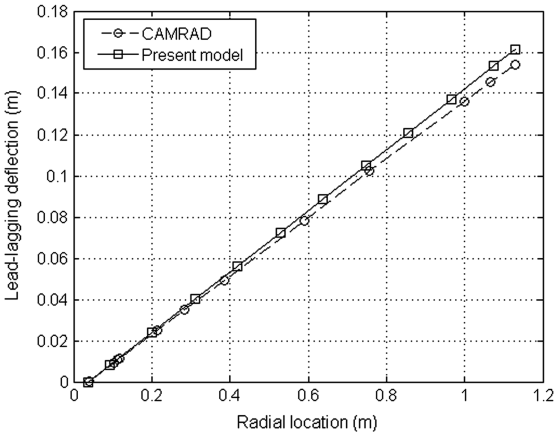

Fig. 13 Blade lead-lagging response in hover; collective pitch is 1.30°.

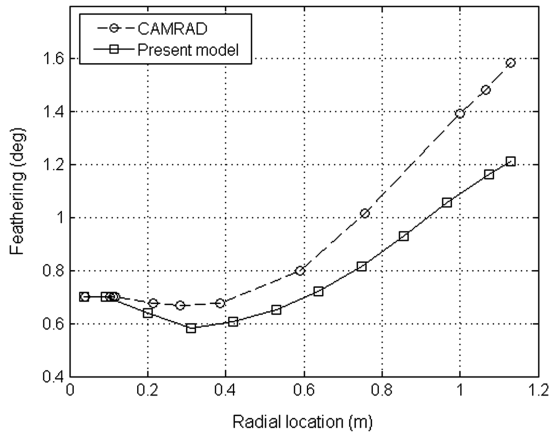

Fig. 14 Blade feathering response in hover; collective pitch is 1.30°.

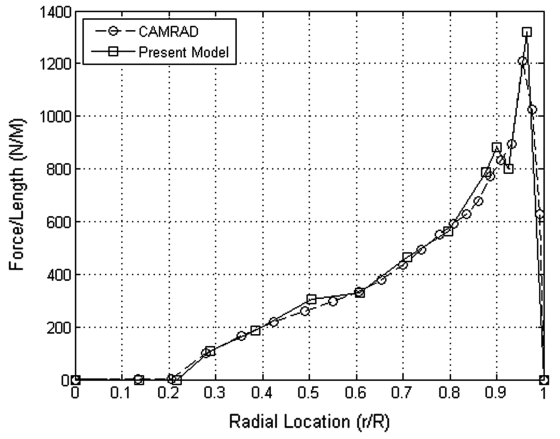

Fig. 15 Spanwise aerodynamic lift distribution in hover; collective pitch is 2°.

C. Blade-Control System Structural Analysis Coupled with Aerodynamic Model

The blade-control system structural analysis was loosely coupled with different aerodynamic models in order to simulate both hover and forward-flight conditions. Aerodynamic models implemented in this paper have been validated in [23]. For the hover condition, the structural model was combined with a free-wake model, which is based on a time-marching, unsteady, source-doublet panel method. The flight conditions considered were hover with a collective pitch of 2° and C_T/σ of 0.066. The external aerodynamic loads (blade sectional lift, drag, and pitching moment) are shown in Figs. 15–17, respectively, and are compared with the results obtained using the free-wake model in CAMRAD II. The loads from the aerodynamic model are in good agreement with CAMRAD II, but have a noticeable discrepancy near the blade tip. The blade flapping and lead-lag response for this flight condition are in good agreement with the results from CAMRAD II (Figs. 18 and 19). The flapping response predicted by the present model is larger than CAMRAD II by approximately 20%. This is because the current free-wake model estimates a higher sectional lift than CAMRAD II. For the lead-lagging deflection, the present results are in good agreement with those by CAMRAD II within 10%.

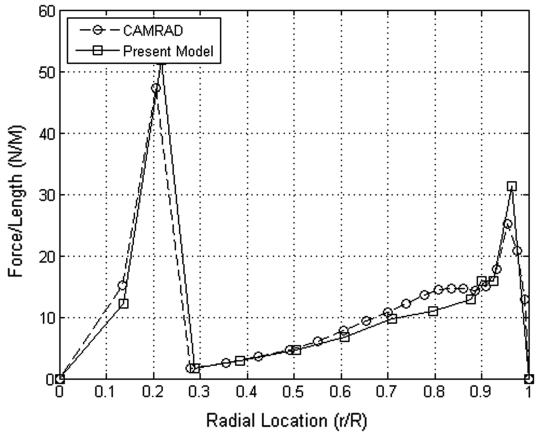

Fig. 16 Spanwise aerodynamic drag distribution in hover; collective pitch is 2°.

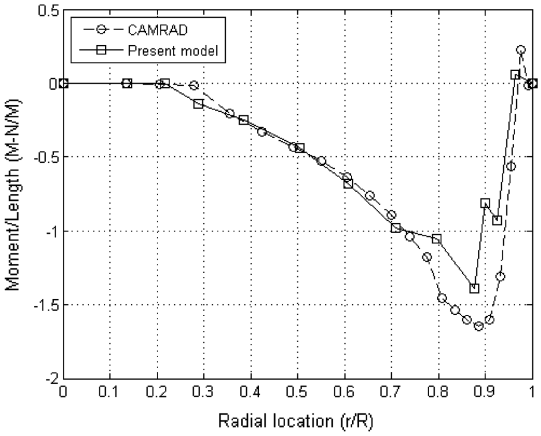

Fig. 17 Spanwise aerodynamic pitching moment distribution in hover; collective pitch is 2°.

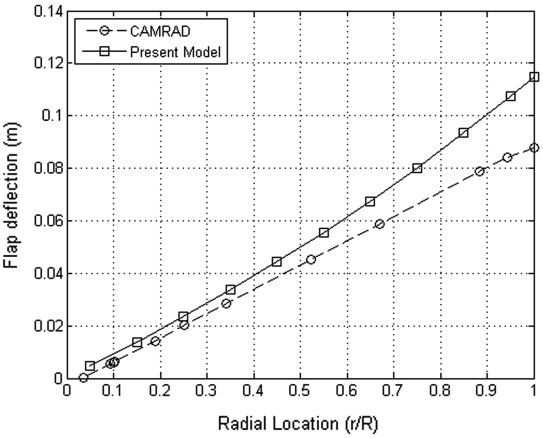

Fig. 18 Blade flapwise response in hover; collective pitch is 2°.

Figure 20 shows the resulting elastic pitch link load for the hover condition. The average pitch link load calculated from the present model was −859 N, and CAMRAD II gave −745 N. The difference is approximately 15%. Since the structural responses are directly related with the external aerodynamic loads, the difference is a result from the sectional lift and drag disagreement. Slight oscillations occur near 180° azimuth, because the wake model produces an impulsive load near 0° azimuth, which causes a structural response when structural-aerodynamic models are coupled.

For forward-flight conditions, the structural model was also loosely coupled with the finite state dynamic inflow model.

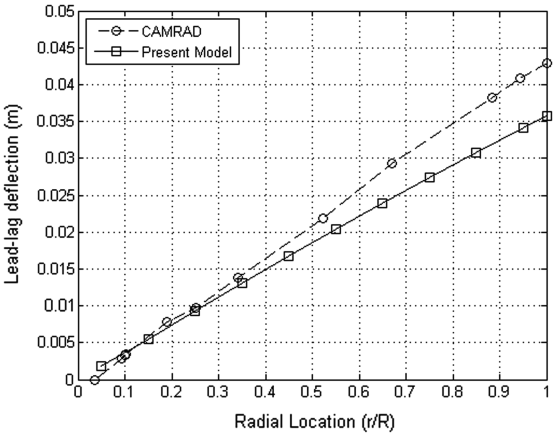

Fig. 19 Blade lead-lag response in hover; collective pitch is 2°.

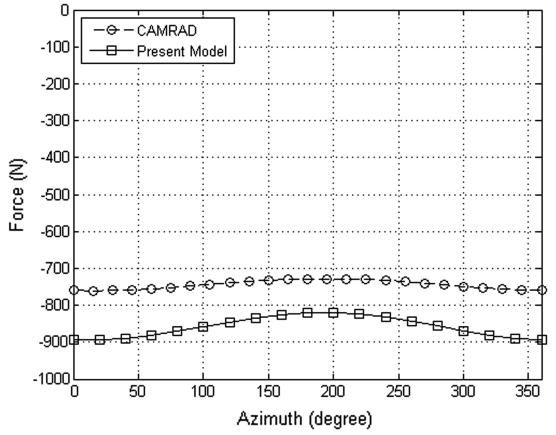

Fig. 20 Elastic pitch link load in hover; collective pitch is 2°.

CAMRAD II was also required to use the same aerodynamic model for validation, but showed a difficulty in analyzing the current blade. Thus, the prescribed wake model was used instead. The flight condition was assumed to be a wind tunnel for forward flight with a μ of 0.1142 and C_T/σ of 0.06633. To compare with regard to the same flight conditions, both CAMRAD II and the model were required to conduct trim analysis. Jacobian trim method was implemented for the trim analysis. The trim results show that the difference between the flight conditions was within 0.3%, shown in Table 3. After the trim analysis was done, the aerodynamic results were compared, especially the sectional lift distribution. Figure 21 shows the prescribed wake results predicted from CAMRAD II, and Fig. 22 shows the results from the finite state dynamic inflow model. The aerodynamic model predicts a slight discrepancy near the blade tip, but is in overall good agreement with both models.

After validating the external loads, blade structural responses were examined. To confirm that the same blade-control inputs are applied to the blades, blade pitch hinge rotation angle was compared, shown in Fig. 23. Since both rotor hub and pitch control modeling are slightly different, a difference in the pitch control inputs is observed. In CAMRAD II, pilot inputs were used for blade pitch control. However, the present model uses geometrical orientations of the swashplate for blade pitch control. Blade deflections were compared at 70% spanwise location along with the azimuthal location.

Table 3 Comparison of the trim results

	CAMRAD II	Present	Difference, %
C_T/σ	0.06633	0.06634	0.01
β_{1C} (°)	0.232015	0.23265	0.3
β_{1S} (°)	−0.497925	−0.49702	0.2

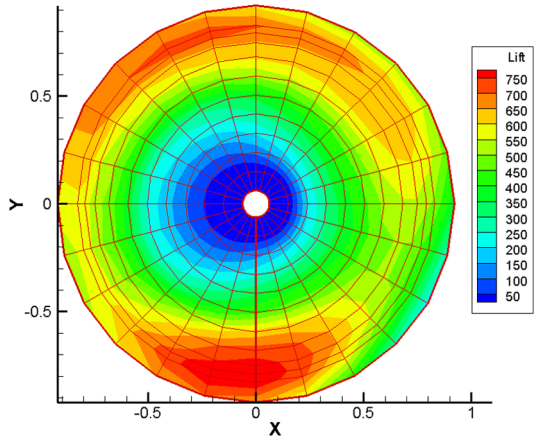

Fig. 21 CAMRAD II: sectional lift result obtained by the prescribed wake model.

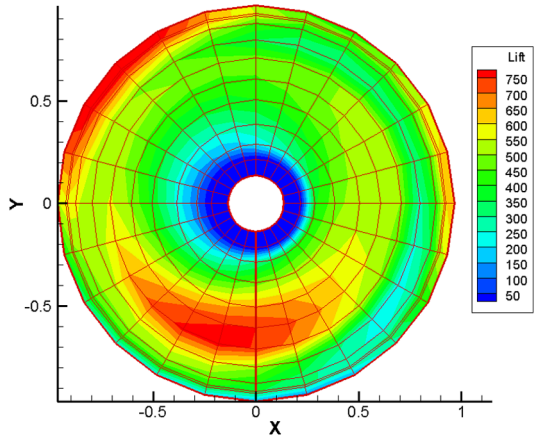

Fig. 22 Present: sectional lift result obtained by the finite state dynamic inflow model.

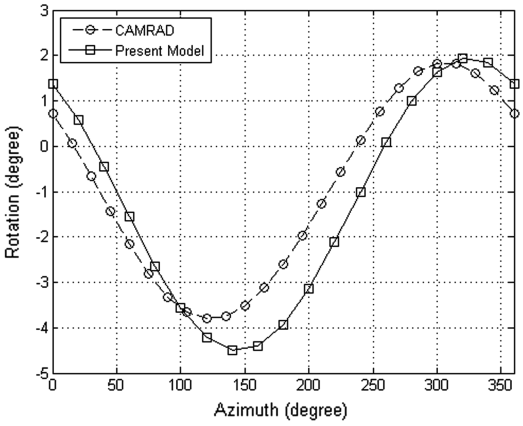

Fig. 23 Control input comparison; pitch hinge rotation angle.

Flapping and lagging deflections match well with those by CAMRAD II with a comparable difference, as shown in Figs. 24 and 25. After the external loads and its structural reactions were validated, the resulting elastic pitch link load in forward-flight condition was compared. In Fig. 26, the elastic pitch link load shows a little shift, but the resulting load amplitude compares well with those from CAMRAD II. Since pitch link loads are mainly related with the pitch link displacement change and its changing rate, the blade pitch hinge rotation angle difference, as shown in Fig. 23, causes a certain shift in the resulting loads.

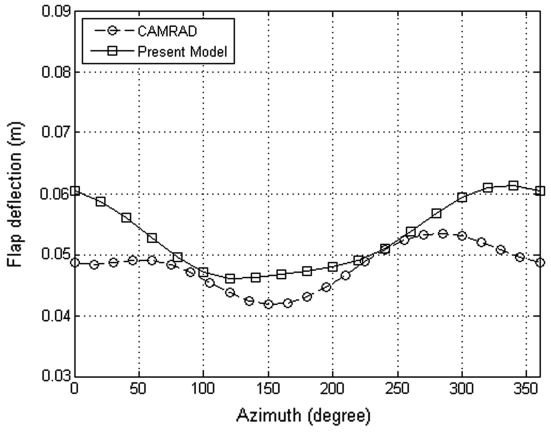

Fig. 24 Blade flapwise response in forward flight.

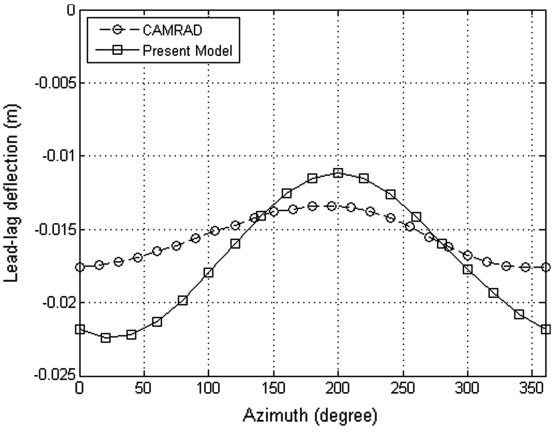

Fig. 25 Blade lead-lagging response in forward flight.

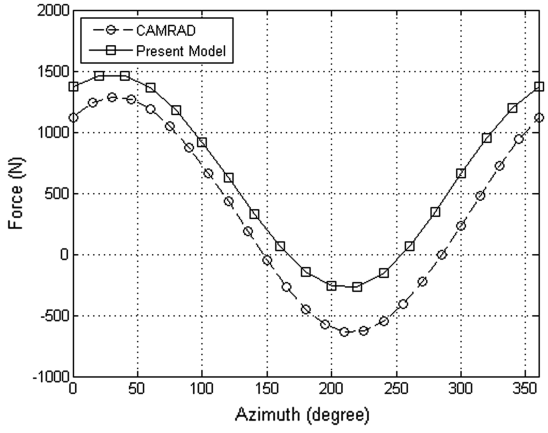

Fig. 26 Elastic pitch link load in forward flight.

It was observed that the present analysis required significantly less amount of effort regarding the input model creation and the consecutive computations when compared with those needed in the existing comprehensive analysis. For example, CAMRAD II required quite a few detailed model parameters for the model creation and required sensitive adjustment of those parameters to obtain a trim solution for each different flight condition. The present analysis featured a similar level of model details and robustness in the trim solution. However, the present analysis still needs to go through a further validation process by comparing with the existing comprehensive programs. Validation using wind-tunnel experimental results is also planned for future studies. The present analysis provides predictions comparable to those of CAMRAD II, and it is

thus concluded that it accomplishes the two following objectives: model compactness and sophistication in analysis capability.

VI. Conclusions

In this study, combination of a geometrically exact beam formulation and a multicomponent analysis for a helicopter rotor was attempted with goals of achieving an accurate prediction of rotor and control system loads. Compared with existing comprehensive rotorcraft analyses, both model compactness and sophistication in the analysis capability are pursued in the present study. In more detail, the rotor blade was modeled using an exact beam analysis based on an intrinsic formulation implemented in time domain. Numerical results for the beam model (without control system) were validated with a multibody dynamics analysis, DYMORE. The rotor control system was modeled as a combination of rigid and elastic bodies. The kinematical relationship between the pitch link elongation, motion of blade root, and swashplate motions were systematically derived. The additional terms in the principle of the virtual work due to the control system components were then included to derive the coupled rotor-blade/control-system aeroelastic model. Numerical results were obtained for a four-bladed, small-scale, articulated rotor 1) rotating in vacuum and 2) hover in a wind tunnel. For case 2, external aerodynamic loads predicted by CAMRAD II were coupled with the structural model. The rotor blade response and pitch link loads were compared with those of CAMRAD II and correlated well. Discrepancies were found in the blade response and are mainly due to the difference in the aerodynamic prediction. Then, the blade-control system structural model was coupled with appropriate aerodynamic models in order to simulate both hover and forward-flight conditions. Numerical results were obtained for a four-bladed, small-scale, articulated rotor in 1) a hover coupled with a free-wake model and 2) forward flight in a wind tunnel coupled with a finite state dynamic inflow model. The rotor blade response and pitch link loads were compared with those of CAMRAD II. The blade response difference was less than 10%, and the correlation is satisfactory. The amplitude of the pitch link load had a difference of approximately 15 and 10% for hover and forward flight, respectively. A larger discrepancy in the forward-flight condition was due to a different type of aerodynamics used between the present analysis and CAMRAD II. Other factors inducing the discrepancies will be examined in the future, including the structural model. In the future by using the same level of aerodynamic model, blade responses and estimated loads will be compared with those of CAMRAD II. After updating the aerodynamic models and validating its results, structural responses will be further investigated. Comparison and validation with wind-tunnel experiments is planned for future studies. Extension into a tight coupling methodology will be also attempted to analyze the maneuvering flight condition of the helicopter.

Acknowledgments

This work has been supported by the Korea Aerospace Research Institute under the Korean Helicopter Program Dual-Use Component Development Program and funded by the Korean Ministry of Knowledge and Economy. This work was also supported by the second stage of the Brain Korea 21 Project in 2007–2008. The authors would like to thank JunBae Lee and Kwanjung Lee from Pusan National University, Korea, for their help and contributions on the aerodynamic models developed in this study.

References

[1] Bielawa, R. L., "Rotating Beams," *Rotary Wing Structural Dynamics and Aeroelasticity*, 2nd ed., AIAA Education Series, Reston, VA, 2006, pp. 67–125.

[2] Friedmann, P. P., "Renaissance of Aeroelasticity and Its Future," *Journal of Aircraft*, Vol. 36, No. 1, 1999, pp. 105–121. doi:10.2514/2.2418

[3] Johnson, W., "Technology Drivers in the Development of CAMRAD II," *Proceedings of the AHS Aeromechanics Specialist Conference*, AHS International, Alexandria, VA, 1994, pp. 3.1–3.14.

[4] Lim, J. W., Yu, Y. H., and Johnson, W., "Calculation of the Rotor Blade-Vortex Interaction Airloads using a Multiple Trailer Free-wake Model," *Journal of Aircraft*, Vol. 40, No. 6, 2003, pp. 1123–1130. doi:10.2514/2.7200

[5] Bir, G. S., Chopra, I., Kim, K. C., Wang, J., Smith, E., Vellaichamy, S., Ganguli, R., Nixon, M., and Torok, S., "University of Maryland Advanced Rotorcraft Code (UMARC) Theory Manual," Univ. of Maryland, Rept. 92-02, College Park, MD, 1992.

[6] Bauchau, O. A., "Dymore User's Manual," Georgia Inst. of Technology, Atlanta, Aug. 2007.

[7] Johnson, W., "Rotorcraft Dynamics Models for a Comprehensive Analysis," *American Helicopter Society 54th Annual Forum* [CD-ROM], AHS International, Alexandria, VA, May 1998.

[8] Johnson, W., "Rotorcraft Aerodynamics Models for a Comprehensive Analysis," *American Helicopter Society 54th Annual Forum* [CD-ROM], AHS International, Alexandria, VA, May 1998.

[9] Hodges, D. H., and Dowell, E. H., "Nonlinear Equations of Motion for the Elastic Bending and Torsion of Twisted Nonuniform Rotor Blades," NASA TN D-7818, Dec. 1974.

[10] Datta, A., and Chopra, I., "Validation of Structural and Aerodynamic Modelling Using UH-60A Airloads Program Data," *Journal of the American Helicopter Society*, Vol. 51, No. 1, Jan. 2006, pp. 43–58. doi:10.4050/1.3092877

[11] Datta, A., Sitaraman, J., Chopra, I., and Baeder, J., "CFD/CSD Prediction of Rotor Vibratory Loads in High-speed Flight," *Journal of Aircraft*, Vol. 43, No. 6, 2006, pp. 1698–1709. doi:10.2514/1.18915

[12] Bauchau, O. A., "Computational Schemes for Flexible Nonlinear Multibody Systems," *Multibody System Dynamics*, Vol. 2, No. 2, 1998, pp. 169–225. doi:10.1023/A:1009710818135

[13] Bauchau, O. A., "DYMORE: A Finite Element Based Tool for the Analysis of Nonlinear Flexible Multibody Systems," Georgia Inst. of Technology, Atlanta, 2001.

[14] Bauchau, O. A., Bottasso, C. L., and Trainelli, L., "Robust Integration Schemes for Flexible Multibody Systems," *Computer Methods in Applied Mechanics and Engineering*, Vol. 192, Nos. 3–4, 2003, pp. 395–420. doi:10.1016/S0045-7825(02)00519-4

[15] Bauchau, O. A., Bottasso, C. L., and Nikishkov, Y. G., "Modeling Rotorcraft Dynamics with Finite Element Multibody Procedures." *Mathematical and Computer Modelling*, Vol. 33, Nos. 10–11, 2001, pp. 1113–1137. doi:10.1016/S0895-7177(00)00303-4

[16] Bauchau, O. A., and Nikishkov, Y. G., "An Implicit Floquet Analysis for Rotorcraft Stability Evaluation," *Journal of the American Helicopter Society*, Vol. 46, No. 3, July 2001, pp. 200–209. doi:10.4050/JAHS.46.200

[17] Peters, D. A., Karunamoorthy, S., and Cao, W. M., "Finite State Induced Flow Models. Part I: Two-Dimensional Thin Airfoil," *Journal of Aircraft*, Vol. 32, No. 2, 1995, pp. 313–322. doi:10.2514/3.46718

[18] Peters, D. A., and He, C. J., "Finite State Induced Flow Models. Part II: Three-Dimensional Rotor Disk," *Journal of Aircraft*, Vol. 32, No. 2, 1995, pp. 323–333. doi:10.2514/3.46719

[19] Berdichevsky, V. L., "Variational-asymptotic Method of Constructing a Theory of Shells," *Journal of Applied Mathematics and Mechanics*, Vol. 43, No. 4, 1979, pp. 664–687. doi:10.1016/0021-8928(79)90152-7

[20] Hodges, D. H., "A Mixed Variational Formulation Based on Exact Intrinsic Equations for Dynamics of Moving Beams," *International Journal of Solids and Structures*, Vol. 26, No. 11, 1990, pp. 1253–1273. doi:10.1016/0020-7683(90)90060-9

[21] Shang, X., "Aeroelastic Stability of Composite Hingeless Rotors with Finite State Unsteady Aerodynamics," Ph.D. Dissertation, School of Aerospace Engineering, Georgia Inst. of Technology, Atlanta, Aug. 1995.

[22] Cheng, T., "Structural Dynamics Modeling of Helicopter Blades for Computational Aeroelasticity," M. S. Dissertation, Dept. of Aeronautics and Astronautics, Massachusetts Inst. of Technology, Cambridge, MA, May 2002.

[23] Lee, J. B., Lee, J. W., Yee, K. J., Oh, S. J., and Kim, D. K., "Development of an Aerodynamic Performance Analysis Module for Rotorcraft Comprehensive Analysis Code," *Journal of the Korean Society for Aeronautical and Space Sciences*, Vol. 35, No. 3, 2009, pp. 224–231.